Distinct trivial phases and topological transitions in an interpolating Aubry-André-Fibonacci p-wave superconducting chain

Feng-Mei Wang,[1,*] Xiao-Hua Yang,[2] Jing Yan,[1] Xiao-Peng Han,[1] Jia Liu,[1,†] and Yan Han[1,‡]

[1] *Shanxi Institute of Science and Technology, shanxi Jincheng 048000, China*
[2] *Shanxi University of Electronic Science and Technology, shanxi Linfen 041000, China*

(Dated: August 19, 2026)

We investigate the topological properties and their evolution with the interpolation parameter in a generalized interpolating Aubry−André−Fibonacci (IAAF) model with p-wave superconducting pairing. Analytical phase boundaries are derived for both the AA and Fibonacci limits. In the AA limit, the system undergoes a transition from a topologically nontrivial superconducting phase to an Anderson-localized trivial phase, while in the Fibonacci limit, it evolves into a topologically trivial superconducting phase composed of multifractal critical states that are extended but non-ergodic. These two trivial phases are thus physically distinct. As the interpolation parameter increases, analytical predictions gradually deviate from numerical results due to the structural change of the chemical potential from a smooth cosine to a discrete step-like modulation. Using the dual-space criterion, we demonstrate that the intermediate regime is not a genuine critical phase but a smooth crossover. Remarkably, near the Fibonacci limit, the phase boundary becomes robust against further increases of the interpolation parameter, demonstrating the protective role of Fibonacci quasiperiodicity. Our results establish a comprehensive theoretical framework for topological phase transitions in interpolated quasiperiodic systems.

Keywords: topological transitions, quasiperiodic systems, Majorana zero modes smooth crossover
PACS: 03.65.Vf, 71.23.Ft, 74.20.-z

1 Introduction

Topological phases of matter have become a frontier in condensed matter physics, focusing on phase transitions among topological states and their associated critical phenomena.[1–3] A key hallmark of these phases is the emergence of zero-energy Majorana fermion states, which manifest as topologically protected Majorana zero modes in p-wave topological superconductors.[4–6] These modes are localized at system boundaries and remain robust against weak disorder,[7] providing an ideal platform for topological quantum computing. [8–17] These modes have been experimentally realized in a variety of platforms, including semiconductor nanowires,[6, 11, 18–20] ultracold atomic systems,[21–26], magnetic atomic chains,[27–31] and conventional superconductor-topological insulator heterojunctions.[32–35] However, strong disorder can destroy the nontrivial superconducting phase and drive the system into a topologically trivial phase.[36]

Disorder effects in one-dimensional topological superconductors have been extensively studied .[37–41] In quasiperiodic lattices, the interplay between order and disorder gives rise to a rich variety of quantum phases.[42–50] Cai et al. demonstrated that quasiperiodic disorder drives a transition from a topologically nontrivial phase to an Anderson-localized phase;[51] Wang et al. further revealed extended critical regions in the parameter space;[52] Liu et al. discovered topologically nontrivial localized phases in slowly varying incommensurate potentials with mobility edges.[42] Among various quasiperiodic models, the AA model[53–55] and the Fibonacci model[56, 57] have emerged as two paradigmatic examples.[58–62] The AA model features cosine modulation of on-site potentials,[63] while the Fibonacci model employs discrete modulation.[64] These two models belong to the same topological class and can be regarded as two limits of the IAAF model.[65–67] This model provides a unified framework for characterizing the topological properties of Fibonacci chains[65, 66, 68] and realizing topological pumping.[66] Guo mainly investigated the quantum phase transitions in this model with p-wave pairing.[69] However, that work focuses primarily on localization properties, revealing rich intermediate phases with coexisting extended, critical, and localized states and relies solely on numerical simulations without providing analytical phase boundaries. In contrast, the topological aspects of the IAAF model remain underexplored, and no analytical topological phase boundary has been established.

It is worth emphasizing that the potential adopted in this work, $V_i(A) = \tanh[A\cos(2\pi\alpha i+\phi)]/\tanh(A)$, differs from that used in Ref.[69], $V_i(\beta) = -\tanh[\beta\cos(2\pi\alpha i + \phi) - \cos(\pi\alpha)]/\tanh(\beta)$. In the AA limit, our potential reduces to a pure cosine modulation without any constant on-site chemical potential shift, so that the model strictly recovers the standard AA p-wave superconductor, whose topological phase boundary admits an exact analytical solution. In contrast, the potential of Ref.[69] contains an additional constant offset $\cos(\pi\alpha)$ in the AA limit, which shifts the topological phase boundary away from the standard value. Consequently, although both models belong to the IAAF family, they are distinct models whose topological phase boundaries differ quantitatively, as we demonstrate numerically in Sec. 4. A subtle issue

* wangfengmei@sxist.edu.cn
† liujia18@sxist.edu.cn
‡ hanyan@sxist.edu.cn

concerns the nature of the intermediate states. The model interpolates between the AA limit (extended or Anderson-localized eigenstates) and the Fibonacci limit (generically critical eigenstates). A natural question then arises: does the intermediate regime host a genuine critical phase or merely a crossover? To address this, we adopt the recently established dual-space criterion: a state is critical if the Lyapunov exponents vanish simultaneously in both real and momentum space , and the inverse participation ratios in the two conjugate spaces exhibit matching scaling behavior.[70–72] We will apply this criterion in Sec. 4 to characterize the intermediate regime.

This work systematically investigates topological quantum phase transitions in the one-dimensional IAAF model with p-wave superconducting pairing. We derive analytical phase boundaries for both the AA and Fibonacci limits and verify them numerically. The system transitions from a topologically nontrivial superconducting phase to an Anderson-localized phase in the AA limit, and to a topologically trivial superconducting phase in the Fibonacci limit. The two trivial phases are fundamentally distinct: the former is Anderson localized, while the latter consists of multifractal critical states. As the interpolation parameter increases, the system gradually deviates from the AA-limit analytical predictions. Using the dual-space criterion, we show that the intermediate regime is a crossover rather than a genuine critical phase. The paper is organized as follows: In Sec. 2, The interpolated Aubry-André-Fibonacci model is presented, followed by an introduction of the Bogoliubov-de Gennes (BdG) theory, and the quantities characterizing the quantum phases and the topological invariant are outlined. In Sec. 3, we investigate the distinct topological properties exhibited in both the generalized Aubry-André and Fibonacci limits. In Sec. 4, we systematically explore the evolution of topological phases ranging from the AA limit to the Fibonacci limit by continuously tuning the interpolation parameter, discuss the validity of the analytical results, and analyze the criticality of the intermediate regime using the dual-space criterion. In Sec. 5, we summarize our main findings and outlook.

2 Model and methods

We consider the one-dimensional generalized interpolated Aubry-André-Fibonacci model with p-wave superconducting pairing, described by the following Hamiltonian

$$\hat{H} = \sum_i \left(-t\hat{c}_i^\dagger \hat{c}_{i+1} + \Delta \hat{c}_i \hat{c}_{i+1} + h.c.\right) + \lambda \sum_i V_i(A)\hat{n}_i, \tag{1}$$

Here i denotes the lattice site index. $\hat{c}_i^\dagger(\hat{c}_i)$ is the creation (annihilation) operator. t is the nearest-neighbor hopping amplitude with $t = 1$ set as an energy unit, Δ is the p-wave pairing amplitude taken to be real and positive, and λ is the amplitude of the quasiperiodically modulated on-site chemical potential. The on-site potential $V_i(A)$ is defined as

$$V_i(A) = \frac{\tanh[A\cos(2\pi\alpha i + \phi)]}{\tanh(A)}. \tag{2}$$

The spatial modulation frequency α is taken as the inverse of the golden mean, obtained from the limit of the ratio of successive Fibonacci numbers with resonance frequency F_n: $\alpha = \lim_{n\to\infty} \frac{F_{n-1}}{F_n} = \frac{\sqrt{5}-1}{2}$ and $F_0 = F_1 = 1$. Without loss of generality, the phase in the quasiperiodic potential is set to zero ($\phi = 0$). A is the interpolation parameter of the quasiperiodic on-site potential, which provides a tuning mechanism enabling the chemical potential to undergo a continuous transition between two known limiting cases. When the Hamiltonian is given by Eq. (1) with $\Delta = 0$, the system reduces to the quasiperiodic model established by Hiramoto and Kohmoto.[73] In this case, when A is small, an extended-localized phase transition occurs; when A takes sufficiently large values, the phase transition behavior becomes complicated, and the position of the mobility edge depends on A. When the Hamiltonian is given by Eq. (1) with $\Delta \neq 0$, if $A \to 0$, the quasiperiodic chemical potential in Eq. (2) simplifies to a standard cosine function, allowing the system to be described by an incommensurate lattice model with p-wave superconducting pairing.[51] If $A \to \infty$, the potential follows the Fibonacci substitution rule, manifesting as a step potential switching between two discrete values of 1.

Due to the particle-hole symmetry of Hamiltonian (1), the BdG transformation can be employed to diagonalize it .[74–76] A set of quasiparticle operators is introduced as follows:

$$\hat{\eta}_n^\dagger = \sum_{i=1}^{L} (u_{ni}\hat{c}_i^\dagger + v_{ni}\hat{c}_i), \tag{3}$$

Here, n represents the energy level index and L is the number of lattice sites, $\hat{\eta}_n$ is the annihilation (creation) operator of quasiparticle. The two components of the wavefunction at the i-th lattice site are denoted as u_{ni} and v_{ni} , which satisfy the normalization condition $\sum_i^L (u_{ni}^2 + v_{ni}^2) = 1$. In terms of the operators, the diagonalized Hamiltonian is written as

$$\hat{H} = \sum_{n=1}^{L} E_n(\hat{\eta}_n^\dagger \hat{\eta}_n - \frac{1}{2}), \tag{4}$$

Here, E_n is the energy spectrum, The quantities u_{ni}, v_{ni} and E_n can be obtained by solving the BdG equations as follows:

$$\begin{pmatrix} \hat{W} & \hat{\Delta} \\ -\hat{\Delta} & -\hat{W} \end{pmatrix} = E_n \begin{pmatrix} u_n \\ v_n \end{pmatrix}. \tag{5}$$

where $\hat{W}_{ij} = -t(\delta_{j,i+1} + \delta_{j,i-1}) + \lambda V_{ij}\delta_{ji}$, $\hat{\Delta}_{i,j} = -\Delta(\delta_{j,i+1} - \delta_{j,i-1})$. The eigenvector components

are defined as $u_n^T = (u_{n1}, u_{n2}, ..., u_{nL})^T$ and $v_n^T = (v_{n1}, v_{n2}, ..., v_{nL})^T$. To quantitatively characterize the topological properties of the system, the eigenvalue equation can be derived from Eq. (5) for $(E_1 = 0)$:

$$\begin{cases} -t(u_{i+1} + u_{i-1}) - \Delta(v_{i+1} - v_{i-1}) + \lambda V_i u_i = 0, \\ t(v_{i+1} + v_{i-1}) + \Delta(u_{i+1} - u_{i-1}) - \lambda V_i v_i = 0. \end{cases} \tag{6}$$

By introducing the two-component wave functions $\phi_{ni} = u_{ni} + v_{ni}$ and $\psi_{ni} = u_{ni} - v_{ni}$, the eigenvalue equation for the zero-energy state of the system can be derived as

$$\begin{cases} -(t + \Delta)\psi_{i+1} + \lambda V_i \psi_i + (\Delta - t)\psi_{i-1} = 0, \\ (\Delta - t)\phi_{i+1} + \lambda V_i \phi_i - (\Delta + t)\phi_{i-1} = 0. \end{cases} \tag{7}$$

Eq. (7) can be expressed in terms of a transfer matrix[77] formalism as:

$$\begin{bmatrix} \psi_{i+1} \\ \psi_i \end{bmatrix} = F_i \begin{bmatrix} \psi_i \\ \psi_{i-1} \end{bmatrix}, \tag{8}$$

where $F_i = \begin{pmatrix} \frac{\lambda V_i(A)}{\Delta + t} & \frac{\Delta - t}{\Delta + t} \\ 1 & 0 \end{pmatrix}$ is the *i-th* transfer matrix, and the total transfer matrix of the system size L is defined as $F = F_L F_{L-1} \cdots F_2 F_1$ with eigenvalues ξ_1 and ξ_2. Assuming $|\xi_1| < |\xi_2|$, the topological invariant can be defined as[43, 78, 79]

$$Q = \mathrm{sgn}(\ln(|\xi_2|)). \tag{9}$$

When $Q = -1$, the system hosts a topologically non-trivial superconducting phase, supporting localized Majorana zero modes (MZMs) at both ends of the system under open boundary conditions. When $Q = 1$, the system remains in a topologically trivial phase with no MZMs present. To characterize the nature of the quasiparticle states beyond the topological invariant, we further introduce the inverse participation ratio (IPR). For the n-th quasiparticle state, the IPR is defined as[80]

$$\mathrm{IPR}^{(n)} = \sum_{i=1}^{L} (|u_{ni}|^4 + |v_{ni}|^4), \tag{10}$$

In the extended state regime, $\mathrm{IPR}^{(n)}$ scales as $1/(2L)$ and thus vanishes($\mathrm{IPR}^{(n)} \to 0$) in the thermodynamic limit $L \to \infty$; while in the localized state regime, the wavefunction is confined to a finite number of lattice sites with the IPR retaining a finite value even as $L \to \infty$. To characterize the localization properties of the system more globally, the average inverse participation ratio ($\langle \mathrm{IPR} \rangle$) is introduced.[69]

$$\langle \mathrm{IPR} \rangle = \frac{1}{2L} \sum_{n=1}^{2L} \mathrm{IPR}_n \tag{11}$$

If the system is in a fully extended phase, it satisfies $\langle \mathrm{IPR} \rangle \sim 1/2L$; while in a completely localized phase, $\langle \mathrm{IPR} \rangle$ remains finite.[69]

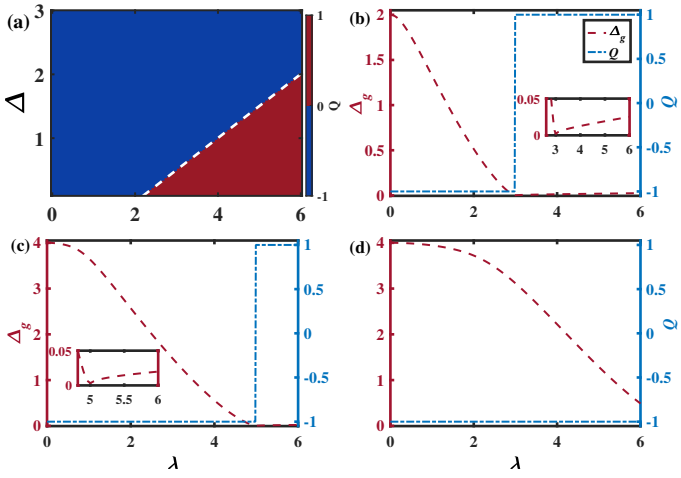


FIG. 1. (a) The $\mathbb{Z}_2$ topological invariant Q as a function of the quasiperiodic modulation strength λ and the pairing strength Δ. The colorbar shows the value of the $\mathbb{Z}_2$ topological invariant Q. The dashed line represents the analytical solution of the topological phase boundary in Eq . (15). Energy gap Δ_g and the $\mathbb{Z}_2$ topological invariant Q as functions of the quasiperiodic modulation strength λ, where $\Delta = 0.5, 1.5, 2.5$ for (b)-(d) under periodic boundary conditions, respectively. The insets in Figs. 1(b) and (c) show magnified views of the region near the energy gap closing point. System parameters are $A = 0.1$, $L = 610$.

3 Topological phase transitions in the AA and Fibonacci limits

3.1 AA limit: analytical phase boundary and Anderson localization

In this subsection, we investigate the topological phase transition characteristics of the system under the limit of a finite small interpolation parameter A. To obtain an analytical solution of the topological phase transition point, we draw on the Taylor expansion method in Ref. [64] to perform an asymptotic approximation on the lattice potential as it approaches the small-parameter limit. To leading order in A, the potential can be approximated by its spatial average over one period, yielding $\lambda V_i(A) \approx \lambda(1 + \frac{A^2}{6})\cos(2\pi\alpha i) = \lambda_{\mathrm{eff}}\cos(2\pi\alpha i)$ with $\lambda_{eff} = \lambda(1 + \frac{A^2}{6})$. This effective-amplitude approximation neglects position-dependent higher-order corrections of $O(A^4)$ and is justified only for sufficiently small A. Under periodic boundary conditions, the Hamiltonian (1) can be re-expressed as

$$\hat{H} = \sum_{ii'} \left[\hat{c}_i^\dagger W_{ii'} \hat{c}_{i'} + \frac{1}{2} \left(\hat{c}_i^\dagger D_{ii'} \hat{c}_{i'}^\dagger + h.c. \right) \right], \tag{12}$$

where W is a symmetric matrix and D is an antisymmetric matrix, with their forms given by

$$W = \begin{pmatrix} \lambda_{eff}V_1 & -t & \cdots & -t \\ -t & \lambda_{eff}V_2 & & \\ \vdots & & \ddots & -t \\ -t & & -t & \lambda_{eff}V_L \end{pmatrix}, \quad (13)$$

$$D = \begin{pmatrix} 0 & -\Delta & \cdots & \Delta \\ \Delta & 0 & & \\ \vdots & & \ddots & -\Delta \\ -\Delta & & \Delta & 0 \end{pmatrix}. \quad (14)$$

The eigenenergies of the system can be obtained by solving the secular equation $\det\left[(W+D)(W-D)-E^2\right]=0$. When a topological phase transition occurs, the energy gap closes, and the corresponding eigenenergy satisfies $E=0$. Therefore, solving the secular equation $\det\left[(W+D)(W-D)\right]=0$ can determine the topological phase transition point.[43, 47, 81] Since $\det(W-D)=\det(W-D)^T=\det(W+D)$, in the thermodynamic limit, the exact topological phase transition condition reduces to solving $\det(W-D)=0$, yielding the topological phase boundary at λ_c as follows

$$\lambda_c(A)=\frac{2(1+\Delta)}{1+\frac{A^2}{6}}. \quad (15)$$

Under periodic boundary conditions, Fig.1 (a) shows that the phase diagram of the topological invariant Q as a function of the p-wave superconducting pairing strength Δ and quasiperiodic chemical potential modulation strength λ with the interpolation parameter $A=0.1$. The color scale represents the magnitude of Q. The blue region corresponds to $Q=-1$, indicating a topologically non-trivial superconducting phase, while the wine-red region corresponds to $Q=1$, indicating a topologically trivial phase. The red dashed line marks the analytical result given in Eq. (15), which defines the topological phase boundary. This boundary separates the topologically nontrivial superconducting phase (blue region) from the topologically trivial phase (wine-red region). When in the case of $\Delta\to 0$, if $\lambda<\lambda_c\approx 2.196$ at $\Delta=0.1$, the system corresponds to a topologically non-trivial superconducting phase and if $\lambda>\lambda_c$, it corresponds to a topologically trivial phase; when $\lambda<6$ and $\Delta>2.005$, the system entirely enters the topologically non-trivial superconducting phase. In the range $0<\Delta<2.005$, the system exhibits a phase transition from a topologically non-trivial superconducting phase to a topologically trivial phase. The analytical results are consistent with the numerical results. In order to precisely characterize this phase transition, we introduce the energy gap $\Delta_g=E_{L+1}-E_L$. Under periodic boundary conditions, the energy gap closes at the topological phase transition points λ_c and reopens when λ exceeds λ_c[42]. Figs.1 (b)-(d) show the evolution of the energy gap Δ_g and

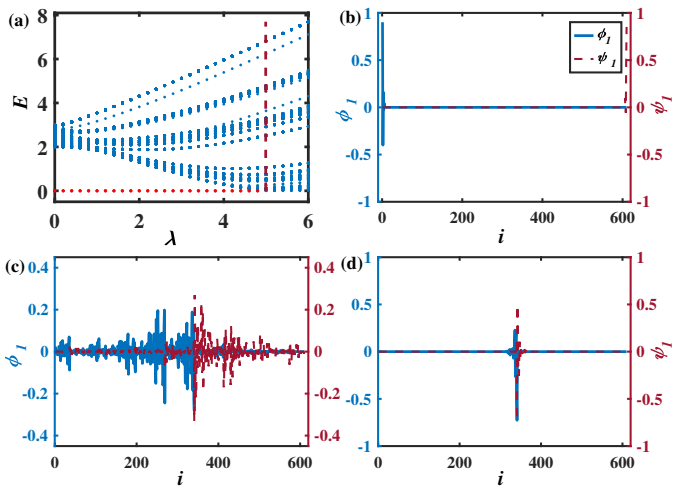


FIG. 2. (a) The eigenenergy E as a function of the quasiperiodic modulation strength λ at $\Delta=1.5$ under open boundary conditions. The dashed line represents the analytical solution of the topological phase boundary in Eq. (15) and the red dots denote the Majorana zero modes. (b)-(d)show the spatial distributions of $\phi_{1,i}$ and $\psi_{1,i}$ for the lowest excitation with $\lambda=1.5, 4.992, 5.8$ for (b)-(d), respectively. System parameters are $A=0.1$, $\Delta=1.5$, $L=610$.

topological invariant Q as functions of the quasiperiodic chemical potential strength λ under periodic boundary conditions (PBC) with the interpolation parameter $A=0.1$. The left vertical axis represents the energy gap Δ_g, while the right vertical axis represents the $\mathbb{Z}_2$ topological invariant Q. Fig.1(b) shows the case of $\Delta=0.5$: the system exhibits a topologically non-trivial superconducting phase with an open energy gap Δ_g and the $\mathbb{Z}_2$ topological invariant $Q=-1$ when $\lambda<\lambda_c\approx 2.995$; the energy gap closes at the critical point $\lambda=\lambda_c$. Conversely, for $\lambda>\lambda_c$, the energy gap reopens, yet the $\mathbb{Z}_2$ topological invariant transitions to $Q=1$, signifying a topologically trivial phase. This stark contrast confirms a phase transition from the non-trivial to the trivial phase at $\lambda_c=2.995$. A similar topological phase transition occurs in Fig.1(c) for $\Delta=1.5$, where the transition point is at $\lambda_c=4.992$. In contrast, Fig.1(d) shows that for the case of $\Delta=2.5$, the energy gap remains persistently open and the $\mathbb{Z}_2$ topological invariant $Q=-1$, indicating the system remains in a topologically non-trivial superconducting phase without any phase transition. These results are fully consistent with the conclusions drawn from Fig.1 (a) , providing comprehensive verification of the phase transition behavior. To further confirm the above conclusions, we present the eigenenergy $E(E>0)$ as a function of the potential strength λ in Fig.2 (a) under open boundary conditions (OBC) with $A=0.1$ and $\Delta=1.5$. The analytically derived phase boundary is marked by the dashed line. Our results demonstrate that Majorana zero modes emerge in the system for λ

values below the critical threshold $\lambda_c \approx 4.992$. When λ exceeds this critical value, Majorana zero modes are absent in the system. To verify this phenomenon, we plot the spatial distributions of the lowest excited states for different values of λ in Figs.2(b)-(d) . Under open boundary conditions, we define $\phi_{1,i} = u_{1,i} + v_{1,i}$, $\psi_{1,i} = u_{1,i} - v_{1,i}$. Fig.2(b) shows the amplitudes of $\phi_{1,i}$ and $\psi_{1,i}$ are localized at the two ends of the system without overlap when $\lambda = 1.5$, forming two spatially independent Majorana edge states. This case corresponds to the topologically non-trivial superconducting phase hosting Majorana zero modes. Fig.2(c) shows that at the critical value $\lambda_c = 4.992$, the amplitudes of $\phi_{1,i}$ and $\psi_{1,i}$ exhibit a certain degree of spatial overlap, signaling the topological phase transition point. In Figs.2(d), for $\lambda = 5.8$, the amplitudes $\phi_{1,i}$ and $\psi_{1,i}$ are completely overlapped and localized at the same spatial position, demonstrating that the zero-energy states are localized fermions.This regime corresponds to the Anderson localized phase, where Majorana zero modes are absent. Taken together, our results confirm that for small finite A, the system undergoes a transition from a topologically non-trivial superconducting phase to an Anderson localized phase, with the numerical results being consistent with the analytical phase boundary Eq. (15).

We emphasize that in the limit $A \to 0$, the potential of Eq. (2) reduces exactly to $\cos(2\pi\alpha i)$ with no constant offset, so that the phase boundary $\lambda_c = 2(t + \Delta)$ of the standard AA p-wave superconductor [51] is recovered from Eq. (15). This exact reduction distinguishes the present model from the shifted potential of Ref. [69], in which the constant offset $cos(\pi\alpha)$ distorts the phase boundary away from $2(t+\Delta)$; we will return to this point in Sec. 4.

3.2 Fibonacci limit: analytical phase boundary and critical states

In this subsection, we investigate the topological phase transition of the system under the limit $A \to \infty$, where the quasiperiodic chemical potential in Hamiltonian (1) transforms into discrete values switching between -1 and 1, making the system equivalent to a p-wave superconductor with Fibonacci quasicrystalline potential modulation. Accordingly, the chemical potential in Eq.(2) can be rewritten as $V_i = \mathrm{sgn}\left[\cos(2\pi\alpha i + \phi)\right]$, where $\mathrm{sgn}(\cdots)$ denotes the sign function. Based on the transfer matrix formalism, the localization length of zero-energy states corresponding to the topologically non-trivial superconducting phase is defined in Refs. [82, 83]

$$\zeta^{-1} = \lim_{L\to\infty} \frac{1}{L} \ln||F||, \tag{16}$$

Here, $||F||$ denotes the norm of the total transfer matrix F. If the localization length exhibits divergent behavior, corresponding to the topological phase transition point, then $\zeta \to \infty$ and $\zeta^{-1} \to 0$ from which the analytical expression of the topological phase transition point can be derived.

$$|\mathrm{Tr}(F)| - \mathrm{Det}(F) = 1. \tag{17}$$

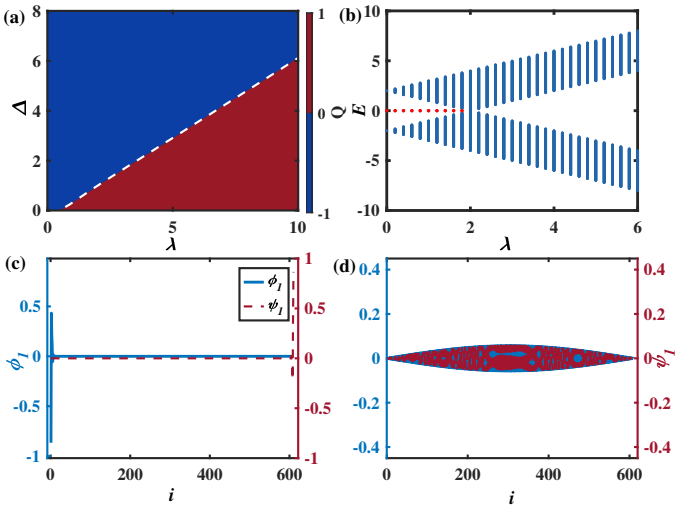


FIG. 3. (a) The $\mathbb{Z}_2$ topological invariant Q as a function of the quasiperiodic modulation strength λ and the pairing strength Δ. The colorbar shows the value of Q. The dashed line indicates the analytically derived phase boundary from Eq. (17). (b)The eigenenergy E as a function of the quasiperiodic modulation strength λ at $\Delta = 1$ under open boundary conditions and the red dots denote the Majorana zero modes. (c)-(d) show the spatial distributions of $\phi_{1,i}$ and $\psi_{1,i}$ for the lowest excitation at $\lambda = 1, 3$, respectively. The pairing strength $\Delta = 1$ for panels (b)-(d). System parameters are $A \to \infty, L = 610$.

Fig.3(a) presents the phase diagram of the $\mathbb{Z}_2$ topological invariant Q as a function of the p-wave superconducting pairing strength Δ and quasiperiodic chemical potential modulation strength λ under open boundary conditions in the limit $A \to \infty$. The magnitude of the $\mathbb{Z}_2$ topological invariant Q is represented by the color scale, with the analytically derived phase boundary from Eq. (17) indicated by the dashed line. In the regime where $\lambda<6$, the system exhibits an abrupt transition from the blue region to the wine-red region with the value of the $\mathbb{Z}_2$ topological invariant Q jumping from -1 to 1, indicating a transition from the topologically non-trivial superconducting phase to the topologically trivial phase. Unlike the case of $A \to 0$, for the same values of Δ and λ, the region of the topologically non-trivial superconducting phase at $A \to \infty$ is significantly narrower. Remarkably, even when $\lambda<6, \Delta>2.005$, the system still exhibits a transition between topologically non-trivial and trivial superconducting phases. Fig.3(b) presents the eigenenergy E as a function of the quasiperiodic modulation strength λ at $\Delta = 1$ under open boundary conditions. It can be clearly observed that when $\lambda<\lambda_c \approx 1.971$, Majorana zero-energy modes exist in the system, whereas when $\lambda>\lambda_c$, the Majorana zero modes disappear and the energy gap opens. This demonstrates that the system undergoes a phase transition from the topologically non-trivial superconducting phase to the

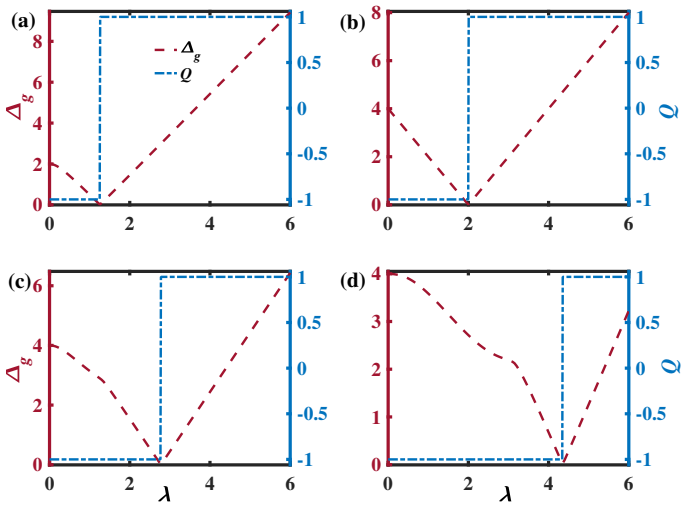


FIG. 4. Energy gap Δ_g and $\mathbb{Z}_2$ topological invariant Q as a function of quasiperiodic modulation strength λ with $\Delta = 0.5, 1, 1.5, 2.5$ for (a)-(d) under periodic boundary conditions, respectively. System parameters are $A \to \infty, L = 610$.

topologically trivial superconducting phase at the energy gap closing point. To verify this phenomenon, Fig.3(c) and 3(d) show the spatial distributions of the lowest excited states for different values of λ indicated in Fig.3(b) under open boundary conditions with $\phi_{1,i} = u_{1,i} + v_{1,i}$ and $\psi_{1,i} = u_{1,i} - v_{1,i}$. In Fig.3(c), when $\lambda = 1$, the amplitudes of $\phi_{1,i}$ and $\psi_{1,i}$ are localized at both ends of the boundary without overlap, forming two spatially independent Majorana edge states that correspond to the topologically non-trivial superconducting phase with Majorana zero modes. In contrast, Fig.3(d) shows the spatial distribution of the lowest excited state with $\lambda = 3$, where the amplitudes of $\phi_{1,i}$ and $\psi_{1,i}$ are distributed throughout the entire space, exhibiting characteristics of critical (multifractal) states that are extended but non-ergodic. This indicates that the corresponding states are not Anderson localized; rather,they correspond to the topologically trivial superconducting phase whose wavefunctions spread over the whole chain while remaining non-ergodic. The critical nature of these states is confirmed by quantitative analysis in Sec. 4.4 . To further confirm this conclusion, Fig.4 presents the calculated energy gap $\Delta_g = E_{L+1} - E_L$ and the $\mathbb{Z}_2$ topological invariant Q as functions of the quasiperiodic chemical potential modulation strength λ under periodic boundary conditions. The left vertical axis represents the energy gap Δ_g while the right vertical axis represents the $\mathbb{Z}_2$ topological invariant Q. Fig.4(a) shows that $\Delta_g > 0$ when $\lambda < \lambda_c \approx 1.250$, indicating an open energy gap with the $\mathbb{Z}_2$ topological invariant $Q = -1$, corresponding to a topologically non-trivial superconducting phase; at $\lambda = \lambda_c$, the energy gap closes and the $\mathbb{Z}_2$ topological invariant Q jumps from -1 to 1. When $\lambda > \lambda_c$, the energy gap reopens with the $\mathbb{Z}_2$ topological invariant $Q = 1$, which corresponds to a trivial superconducting phase. For the case $\Delta = 0.5$, the system undergoes a transition from a nontrivial superconducting phase to topologically trivial superconducting phase at the energy gap closing point. Figs.4(b)−(d) show that for $\Delta = 1, 1.5, 2.5$, respectively, the system exhibits phase transitions qualitatively similar to those in Fig.4(a) , with the critical transition points increasing successively in magnitude. Remarkably, even for $\Delta = 2.5$, the system maintains the characteristic topological phase transition from a non-trivial to trivial superconducting phase. These results provide conclusive verification of the phase diagram conclusions presented in Fig.3(a) .

In summary, topological phase transitions exist in both the $A \to \infty$ and $A \to 0$ limits, but they are fundamentally distinct. For $A \to 0$, the system transitions from the topologically non-trivial superconducting phase to the Anderson localized phase. In contrast, for $A \to \infty$, it transitions from the topologically non-trivial superconducting phase to the topologically trivial superconducting phase without entering an Anderson localized regime; the trivial phase there consists of critical (multifractal) states.

4 Fate of topological quantum phase transitions with increasing A

For the standard IAAF model, the system exhibits distinct topological phase transitions as the interpolation parameter A increases. To investigate how the interpolation parameter A influences these transitions, we systematically analyze the behavior under different parameter conditions. This section is organized as follows: we first discuss the validity range of the analytical results for small A (Sec. 4.1), then analyze the origin of the deviations at intermediate A (Sec. 4.2), and finally examine the robustness and convergence to the Fibonacci limit for large A (Sec. 4.3). In Sec. 4.4, we analyze the criticality of the intermediate regime using the dual-space criterion, and in Sec. 4.5 we explicitly compare our results with those of the interpolating model of Ref. [69].

4.1 Validity of the analytical results for small A

Fig.5(a) presents the integrated phase diagram of the $\mathbb{Z}_2$ topological invariant Q with respect to the parameter A and the modulation strength λ of the quasiperiodic chemical potential for $\Delta = 1$, which now merges the previously separate phase diagrams for small (moderate) A and for large A into a single figure. Based on our results in the limit of infinitesimal A, the system possesses an analytical topological phase boundary when $A \to 0$. The dashed line in Fig.5(a) represents this analytical topological phase boundary given by Eq.(15), which separates the topologically nontrivial superconducting phase (blue region) from the topologically trivial phase (wine-red region). For relatively small values of A, the numerical results show excellent agreement with the analytical predictions. To quantify this agreement, we compute the topological

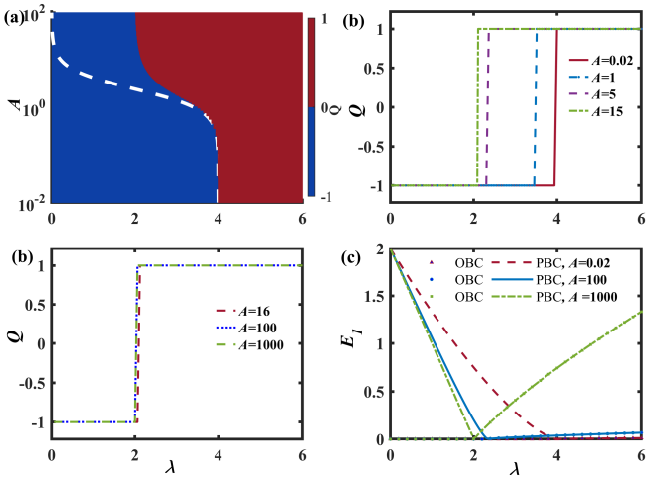


FIG. 5. (a) The $\mathbb{Z}_2$ topological invariant Q as a function of the quasiperiodic modulation strength λ and the interpolation parameter A. The colorbar shows the value of $\mathbb{Z}_2$ topological invariant Q. The dashed line represents the analytical solution of the topological phase boundary in Eq. (15). (b)-(c) The $\mathbb{Z}_2$ topological invariant Q as a function of λ. (d) The lowestexcitation energies E_1 as a function of λ under periodic boundary conditions and under open boundary conditions. Panels (b)-(d) correspond to different A values as indicated. System parameters are $\Delta = 1$ for (b)-(d), and $L = 610$.

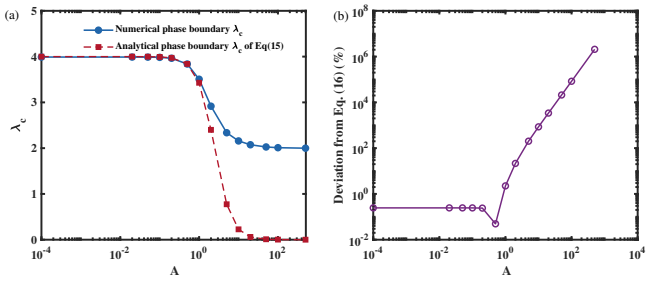


FIG. 6. (a) The topological phase boundary λ_c as a function of the interpolation parameter A at $\Delta = 1$: numerical results from the transfer-matrix invariant Eq. (9) (circles) versus the analytical prediction of Eq. (15) (squares). (b) Relative deviation of the numerical boundary from the analytical prediction, showing the validity range of Eq. (15) for $A \lesssim 0.5$, $L = 610$.

phase boundary $\lambda_c(A)$ from the transfer-matrix invariant [Eq.(9)] and compare it with the analytical prediction of Eq. (15). As shown in Fig.6(a), for $A \lesssim 0.5$ the numerical boundary coincides with the analytical curve within 0.3% [Fig.6(a)], confirming the validity of Eq.(15) in the small-A regime. For $A = 1$, the deviation reaches about 2%. We note that the exact Taylor expansion of Eq. (2) contains position-dependent higher-order corrections, $\tanh[A\cos(2\pi\alpha i)]/\tanh(A) = \cos(2\pi\alpha i) + \frac{A^2}{3}\cos(2\pi\alpha i)\sin2(2\pi\alpha i) + O(A^4)$; the effective amplitude approximation leading to Eq. (15) is therefore justified only to leading order in A, which is consistent with the observed accuracy.

4.2 Origin of the deviations at intermediate A

As A increases, the analytical results begin to deviate from the numerical predictions [see Fig.6(b)], and the deviation grows rapidly once $A \geq 1$. This deviation originates from the fundamental change of the chemical potential structure: with increasing A, the smooth cosine modulation of the AA limit is progressively deformed into the discrete step-like modulation of the Fibonacci limit [see Eq.(2)]. Within the effective-amplitude picture, the leading-order analytical boundary Eq.(15) cannot capture the emergent non-cosine structure, so the deviation reflects the structural transition of the on-site potential rather than a numerical artifact. This interpretation is corroborated by the observation that the phase transition point from the topologically nontrivial superconducting phase to the topologically trivial phase gradually shifts to lower values of λ as A increases. When $A = 0.02$, the phase transition point attains a relatively large value, whereas at $A = 1, 5, 15$, it reaches a comparatively small value [Fig.5(b)]. This conclusion is further supported by examining the lowest excited state energy E_1. Under the same parameters value A as in Fig.5(b), we plot E_1 as a function of the quasiperiodic chemical potential modulation strength λ for both periodic and open boundary conditions in Fig.5(d). Below the topological phase transition point, the system exhibits a finite energy gap under periodic boundary conditions but hosts Majorana zero modes under open boundary conditions. The transition occurs when the energy gap closes (periodic boundary conditions) and the Majorana zero modes vanish (open boundary conditions). This behavior, along with the variation of the transition points in Figs.5(b) and 5(d), aligns with previous conclusions.

4.3 Robustness and convergence to the Fibonacci limit for large A

To further investigate the topological properties of the system for the larger values of the interpolation parameter A, we focus on the large A part of the integrated phase diagram Fig.5(a) and the Q–λ cuts shown in Fig.5(c). For the larger A, the phase boundary separating the topologically nontrivial superconducting phase from the topologically trivial phase remains approximately constant as A increases. As an example, Fig.5(c) illustrates the variation of the $\mathbb{Z}_2$ topological invariant Q with the quasiperiodic chemical potential modulation strength λ for $A = 16, 100$, and 10000. The jump of the topological invariant from -1 to 1 occurs at nearly the same λ for different values of A, confirming a robust phase transition boundary. In Fig.5(d), we show the energy E_1 of the lowest excited state as a function of λ under periodic and open boundary conditions. When $\lambda<\lambda_c \approx 2$, the energy gap remains open under periodic boundary conditions, while Majorana zero-energy modes

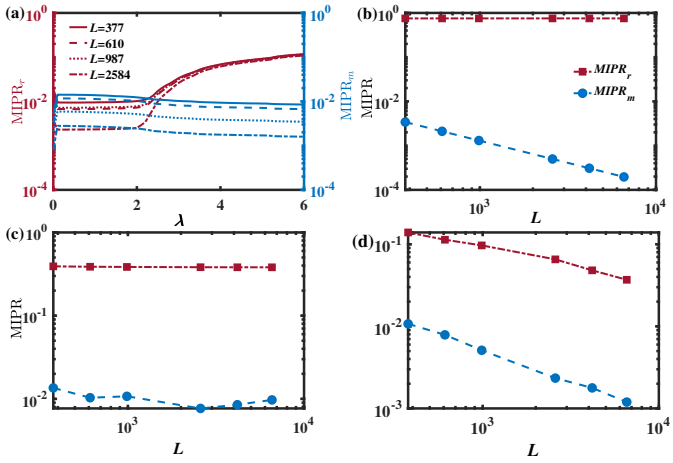


FIG. 7. (a) The real-space mean inverse participation ratio ($\mathrm{MIPR_r}$)(wine-red) and momentum-space mean inverse participation ratio ($\mathrm{MIPR_m}$)(blue) as functions of the quasiperiodic modulation strength λ for various system sizes L at the intermediate interpolation parameter $A = 5$. (b)-(d) The double-logarithmic scaling of the real-space $\mathrm{MIPR_r}$ (red) and momentum-space $\mathrm{MIPR_m}$ (blue) with system size L for three representative cases: (b)the AA limit ($A = 0.02$), (c)the intermediate interpolation ($A = 5$), and (d) the Fibonacci limit($A \to \infty$) with $\lambda = 5$; System parameters are $\Delta = 1, L = 610$.

exist under open boundary conditions. For $\lambda > \lambda_c$, the energy gap reopens and Majorana zero modes disappear, confirming topological phase transitions at $\lambda_c \approx 2$ for both cases. These results demonstrate that increasing A beyond a certain range has little effect on the system's topological phase transitions. This is because a larger value of A drives the system closer to the Fibonacci quasicrystal structure, whose topological properties are inherently insensitive to A due to the robustness of the quasicrystalline symmetry. As shown in Fig. 6(a), the numerical boundary $\lambda_c(A)$ saturates to $\lambda_c \approx 2$ for $A \gtrsim 10$, approaching the analytical condition of Eq.(17) in the Fibonacci limit. This robustness is the "protective role" of the Fibonacci structure: the topological phase boundary becomes insensitive to the interpolation parameter once the potential is sufficiently close to the Fibonacci step potential.

4.4 Nature of the states in the intermediate regime: critical phase or crossover?

Because the model interpolates between the AA limit (extended and Anderson-localized states) and the Fibonacci limit (generically critical states), a natural question is whether the intermediate regime hosts a genuine critical phase. To address this question, we investigate the mean inverse participation ratios (MIPR) in real and momentum spaces as well as their finite-size scaling behavior. According to the recently proposed dual-space criterion,[70–72] a state is identified as critical if it lacks finite exponential localization lengths in both Fourier-conjugate representations.

Fig.7(a) presents the real-space mean inverse participation ratio ($\mathrm{MIPR_r}$, wine-red) and momentum-space mean inverse participation ratio ($\mathrm{MIPR_m}$, blue) as functions of the quasiperiodic modulation strength λ for various system sizes L at the intermediate interpolation parameter $A = 5$. A clear disparity is observed between the evolution of $\mathrm{MIPR_r}$ and $\mathrm{MIPR_m}$ with λ. For large λ, all curves of the real-space $\mathrm{MIPR_r}$ for different system sizes nearly collapse onto a single line and barely vary with L , which indicates that the real-space wavefunctions exhibit size-independent localization features. In contrast, the momentum-space $\mathrm{MIPR_m}$ displays a pronounced size dependence, decreasing systematically as L increases. This distinctively different size dependence between real and momentum spaces is inconsistent with the "simultaneous delocalization in both spaces" characteristic expected for critical states, suggesting that the intermediate regime may not host a genuine critical phase. To further clarify the nature of the eigenstates in the intermediate region, we fix the parameters $\lambda = 5$ and $\Delta = 1$, and compute the double-logarithmic scaling of the real-space $\mathrm{MIPR_r}$ (wine-red) and momentum-space $\mathrm{MIPR_m}$ (blue) with system size L for three representative cases: the AA limit ($A = 0.02$), the intermediate interpolation ($A = 5$), and the Fibonacci limit ($A \to \infty$), as shown in Figs.7(b)−7(d). In the AA limit[Fig.7(b)], the real-space $\mathrm{MIPR_r}$ does not decay with L and remains finite, whereas the momentum-space $\mathrm{MIPR_m}$ decays as L increases. This behavior is consistent with Anderson localization: the real-space wavefunction is exponentially localized, while in momentum space it appears extended. In the Fibonacci limit [Fig.7(d)], both the real-space and momentum-space MIPR exhibit similar power-law decay with L, displaying analogous scaling behaviors with neither showing exponential localization, a hallmark of multifractal critical states. In the intermediate regime [Fig.7(c)], the real-space $\mathrm{MIPR_r}$ remains nearly constant as L increases, while the momentum-space $\mathrm{MIPR_m}$ decays with L. This scaling behavior closely resembles that of the Anderson-localized states in the AA limit, and stands in marked contrast to the critical behavior observed in the Fibonacci limit, where both spaces exhibit concurrent decay. Therefore, the eigenstates in the intermediate regime are not genuine critical states.

In summary, the states in the intermediate regime display size-independent localization in real space and size-dependent extension in momentum space, scaling behaviors consistent with Anderson localization rather than with the dual-space delocalization criterion for criticality. Consequently, the intermediate regime does not constitute a genuine critical phase, but rather a smooth crossover between Anderson-localized and critical behaviors. This crossover arises from the structural transformation of the potential from a smooth cosine modulation to a discrete step-like form, rather than being a finite-size effect.

4.5 Comparison with the interpolating model of Ref. [69]

Given that Ref.[69] studies the same family of interpolating models, we briefly clarify the differences and connections. First, the two models differ in the on-site potential: our potential Eq. (2) has no constant on-site chemical potential offset in the AA limit, whereas the potential of Ref.[69] carries an additional constant offset $\cos(\pi\alpha)$. As a consequence, in the AA limit our topological boundary is given approximately by $\lambda_c(A) = \frac{2(1+\Delta)}{1+\frac{A^2}{6}}$, within the effective-amplitude approximation, which is accurate to leading order in A, while that of Ref.[69] is distorted away from $\lambda_c(A)$; For instance, at $\Delta = 0.5, A = 0.1$, we find $\lambda_c(A) \approx 2.995$ for our model and $\lambda_c(A) \approx 1.9$ for the model of Ref.[69], consistent with the statement in Ref.[69] that its transition point is less than $2(1 + \Delta)$. In the Fibonacci limit, both models approach the same step-potential form and thus share the same saturating boundary $\lambda_c(A) \approx 2$ at $\Delta = 1$. Second, the focus of Ref.[69] is on the localization properties:extended, critical, and localized pure phases as well as multiple intermediate phases with mobility edges, and all its conclusions are drawn from purely numerical calculations, whereas our work focuses on the topological phase transitions, providing analytical phase boundaries [Eqs. (15) and (17)], demonstrating the distinct physical nature of the two trivial phases , revealing the mechanism of the analytical-numerical deviation, and demonstrating the protective role of the Fibonacci structure. Moreover, using the recently proposed dual-space criterion, we show that the intermediate regime corresponds to a smooth crossover between Anderson-localized and critical behaviors rather than a genuine critical phase. These results are complementary to those for the model of Ref.[69] rather than duplicative.

5 Summary and outlook

We have systematically investigated the topological quantum phase transitions in a one-dimensional generalized interpolating Aubry-André-Fibonacci model with p-wave superconducting pairing. Analytical topological phase boundaries are derived for both the AA and Fibonacci limits and verified numerically. In the AA limit, where the on-site potential is a pure cosine modulation, all eigenstates in the topologically trivial phase exhibit localized characteristics, hence, the system enters an Anderson-localized trivial phase. In the Fibonacci limit, the potential reduces to a discrete two-step form; the quasicrystalline structure keeps all eigenstates multifractal and critical, so the system evolves into a topologically trivial superconducting phase composed of extended but non-ergodic critical states—the two trivial phases are fundamentally distinct in wavefunction localization. As the interpolation parameter increases, the potential gradually deforms from a smooth cosine to a step-like form, rendering the effective-amplitude approximation used in the analytical derivation inaccurate, which causes the analytical boundary to gradually deviate from numerical results; this deviation originates from the position-dependent higher-order corrections in the Taylor expansion of the potential. Using the dual-space criterion, we demonstrate that the states in the intermediate regime do not decay with system size in real space but decay with increasing size in momentum space, failing to satisfy the dual-space delocalization criterion for criticality; hence the intermediate regime is a smooth crossover rather than a genuine critical phase. Near the Fibonacci limit, the potential approaches the two-step form, and its quasicrystalline symmetry is robust, making the phase boundary insensitive to further changes in the interpolation parameter and demonstrating the protective role of Fibonacci quasiperiodicity. This work establishes a new theoretical framework for topological phase transitions in interpolated quasiperiodic systems. Future directions include investigating interaction effects on the intermediate phases, introducing non-Hermitian extensions, and generalizing the model to higher dimensions.

Acknowledgments

This work is supported by the National Natural Science Foundation of China (Grant No. 11547134), Fundamental Research Program of Shanxi Province (Grant No. 202203021211337), the Scientific and Technological Innovation Programs of Higher Education Institutions in Shanxi (Grant No. 2025L165), Scientific Research Foundation for Advanced Talents of Shanxi Institute of Science and Technology (Grant Nos. 2024017, 2024010).

APPENDIX: Differences and Innovations Compared with Ref.[69]

This appendix systematically clarifies the essential differences and core innovations of the present work compared with the closely related study in Ref.[69], eliminating the similarity concern and highlighting the unique contributions of our research.

1. Difference in Main Research Line and Physical Connotation of Trivial Phases

Ref.[69] takes localization phase transition as the core research, centering on the classification of pure extended or localized phases and multiple intermediate coexisting phases with mobility edges in the IAAF model, while its discussion of topological properties is only supplementary and lacks in-depth exploration, and relies entirely on numerical simulations without any analytical treatment. In contrast, the present work regards topological quantum phase transition as the central focus, and further distinguishes the physical nature of topologically trivial phases in three parameter intervals, which is not involved in Ref.[69]: (1) In the AA limit, the trivial phase belongs to the typical Anderson localized phase with exponentially localized wavefunctions; (2) In the intermediate parameter region, the system exhibits a smooth crossover state between localization and criticality; (3) In the Fibonacci limit, the

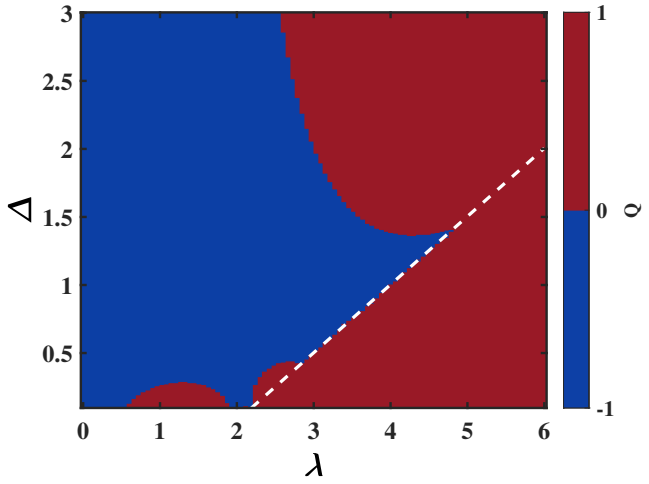


FIG. 8. (a) The $\mathbb{Z}_2$ topological invariant Q as a function of thequasiperiodic modulation strength λ and pairing strength Δ of Ref. [69]. The colorbar shows the value of $\mathbb{Z}_2$ topological invariant Q. The dashed line represents the analytical solution of the topological phase boundary in Eq. (15)[$\lambda_c(A) = 2(1+\Delta)/(1+\frac{A^2}{6})$]. System parameter is $\beta = 0.1$, $L = 610$.

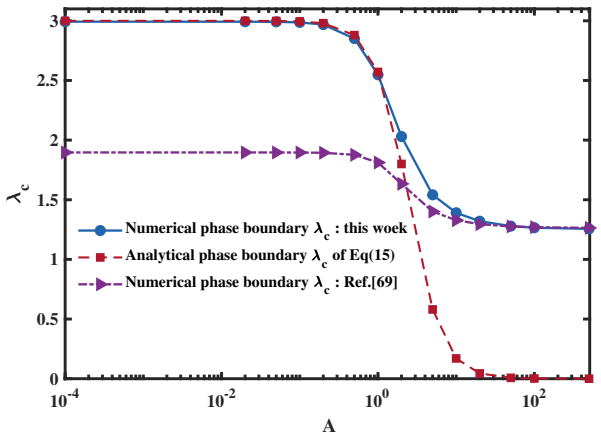


FIG. 9. (a) The topological phase boundary λ_c as a function of the interpolation parameters A at $\Delta = 1$: numerical results from the transfer-matrix invariant (circles) of this work and (triangle) versus the analytical prediction of Eq. (15) (squares). $L = 610$.

trivial phase is a multifractal critical state with extended but non-ergodic features. This classification deepens the physical topologically of trivial topological phases in quasiperiodic superconducting systems.

2. Essential Difference in Model Potential

The two studies adopt fundamentally different on-site quasiperiodic potentials, which is the root cause of quantitative differences in physical results. The potential adopted in this work is $V_i(A) = \tanh[A\cos(2\pi\alpha i + \phi)]/\tanh(A)$, which has no constant chemical potential offset in the AA limit and strictly restores the standard p-wave superconducting AA model, with the topological phase boundary approximately conforming to the theoretical standard value $\lambda_c(A) = 2(1+\Delta)/(1+\frac{A^2}{6})$ within the leading-order effective-amplitude approximation[see Fig.8]. In contrast, the potential in Ref.[69]($V_i(\beta) = -\tanh[\beta\cos(2\pi\alpha i + \phi) - \cos(\pi\alpha)]/\tanh(\beta)$) contains an additional constant offset $\cos(\pi\alpha)$ in the AA limit. This inherent offset distorts the topological phase boundary, making its critical value significantly lower than the standard theoretical result (e.g., $\Delta = 0.5$ our model gives $\lambda_c(A) \approx 3.0$ while Ref.[69] $\lambda_c(A) \approx 1.9$)[see Fig.9]. Although both models belong to the IAAF family, they are physically distinct models with different phase transition characteristics.

3. Analytical Solution of Topological Phase Boundary and Deviation Mechanism

A key innovation of this work is the derivation of exact analytical topological phase boundaries for both AA and Fibonacci limits, which is completely absent in Ref.[69] that only relies on pure numerical simulation. Specifically, we obtain the analytical boundary formula for the AA limit and the transfer matrix critical condition for the Fibonacci limit, and verify that the analytical results maintain high accuracy (deviation $< 0.3\%$) in the small parameter regime ($A \lesssim 0.5$). Furthermore, we reveal the physical mechanism underlying the deviation between analytical predictions and numerical results as the interpolation parameter A increases. This deviation originates from the structural deformation of the on-site potential: the quasiperiodic chemical potential evolves from a smooth cosine modulation in the AA limit to a discrete step-like modulation in the Fibonacci limit, which invalidates the leading-order Taylor expansion approximation and gradually increases the numerical deviation. This physical interpretation fills the research gap in Ref.[69].

4. Characterization of the Intermediate Regime via the Dual-Space Criterion

Based on the recently proposed real/Fourier dual-space criticality criterion and finite-size scaling analysis of the mean inverse participation ratio (MIPR), this work clarifies the nature of the intermediate parameter regime, resolving the unresolved problem in Ref.[69]. The numerical results confirm that the intermediate regime does not satisfy the dual-space simultaneous delocalization characteristic of genuine critical phases: the real-space wavefunction exhibits size-independent localization features, while the momentum-space wavefunction shows obvious size-dependent extension behavior. Therefore, the intermediate regime is only a smooth crossover between Anderson localization and multifractal criticality, rather than a new genuine critical phase. In addition, we verify the protective effect of Fibonacci quasiperiodicity: the topological phase boundary tends to saturate and becomes robust against the variation of interpolation parameters near the Fibonacci limit, which is another

unique conclusion of this work.

References

[1] Stone M and Chung S-B 2006 *Phys. Rev. B* **73** 014505
[2] Qi X L and Zhang S C 2011 *Rev. Mod. Phys.* **83** 1057
[3] Ivanov D A 2001 *Phys. Rev. Lett.* **86** 268
[4] Hasan M Z and Kane C L 2010 *Rev. Mod. Phys.* **82** 3045
[5] Fu L and Kane C L 2008 *Phys. Rev. Lett.* **100** 096407
[6] Lutchyn R M, Sau J D and Das Sarma S 2010 *Phys. Rev. Lett.* **105** 077001
[7] Potter A C and Lee P A 2010 *Phys. Rev. Lett.* **105** 227003
[8] Nayak C, Simon S H, Stern A, Freedman M and Das Sarma S 2008 *Rev. Mod. Phys.* **80** 1083
[9] Sau J D, Tewari S, Lutchyn R M, Stanescu T D and Das Sarma S 2010 *Phys. Rev. B* **82** 214509
[10] Aguado R and Kouwenhoven L P 2020 *Phys. Today* **73** 44
[11] Oreg Y, Refael G and Von Oppen F 2010 *Phys. Rev. Lett.* **105** 177002
[12] Das Sarma S, Freedman M and Nayak C 2005 *Phys. Rev. Lett.* **94** 166802
[13] Mourik V, Zuo K, Frolov S M, Plissard S R, Bakkers E P A M and Kouwenhoven L P 2012 *Science* **336** 1003
[14] Zhao X M, Guo C X, Yang M L, Wang H, Liu W M and Kou S P 2021 *Phys. Rev. B* **104** 214502
[15] Zhao X M, Guo C X, Kou S P,Zhuang L and Liu W M 2021 *Phys. Rev. B* **104** 205131
[16] Beenakker C W J 2013 *Annu. Rev. Condens. Matter Phys.* **4** 113
[17] Yokomizo K and Murakami S 2019 *Phys. Rev. Lett.* **123** 066404
[18] Lu X C and Sénéchal D 2018 *Phys. Rev. B* **98** 245118
[19] Peng L, Naritsuka M, Akutagawa S, Suetsugu S, Haze M, Kasahara Y, Terashima T, Peters R, Matsuda Y and Asaba T 2023 *Phys. Rev. B* **107** L041101
[20] Sajilesh K P, Motla K, Meena P K, Kataria A, Patra C, Somesh K, Hillier A D and Singh R P 2022 *Phys. Rev. B* **105** 094523
[21] Ruhman J, Berg E and Altman E 2015 *Phys. Rev. Lett.* **114** 100401
[22] Hübener H, Sentef M A, Giovannini U D, Kemper A F and Rubio A 2017 *Nat. Commun.* **8** 13940
[23] Qu C L, Zheng Z, Gong M, Xu Y, Mao L, Zou X B, Guo G C and Zhang C W 2013 *Nat. Commun.* **4** 2710
[24] Cheng Q Q, Pan Y M, Wang H Q, Zhang C S, Yu D, Gover A, Zhang H J, Li T, Zhou L and Zhu S N 2019 *Phys. Rev. Lett.* **122** 173901
[25] Chen C 2013 *Phys. Rev. Lett.* **111** 235302
[26] Čadež T, Mondaini R and Sacramento P D 2019 *Phys. Rev. B* **99** 014301
[27] Kim H, Palacio-Morales A, Posske T, Rózsa L, Palotás K, Szunyogh L, Thorwart M and Wiesendange R 2018 *Sci. Adv.***4** eaar5251
[28] Schneider L, Beck P, Rózsa L, Posske T, Wiebe J and Wiesendanger R 2023 *Nat. Commun.* **14** 2742
[29] Pawlak R, Kisiel M, Klinovaja J, Meier T, Kawai S, Glatzel T, Loss D and Meyer E 2016 *npj Quantum Inf* **2** 16035
[30] Jeon S, Xie Y L, Li J, Wang Z J, Bernevig A B and Yazdani A 2017 *Science* **358** 772
[31] Schneider L, Beck P, Posske T, Crawford D, Mascot E, Rachel S, Wiesendanger R and Wiebe J. 2021 *Nat. Phys.* **17** *943*
[32] Legner H F, Loss D, Daniel Loss and Klinovaja J 2023 *Phys. Rev. Lett.* **130** 207001
[33] Hell M, Leijnse M and Flensberg K 2017 *Phys. Rev. Lett.* **118** 107701
[34] Tanaka Y, Sato M and Nagaosa N 2012 *J. Phys. Soc. Jpn.* **81** 011013
[35] Pientka F, Keselman A, Berg E, Yacoby A, Stern A and Halperin B I 2017 *Phys. Rev. X* **7** 021032
[36] Altland A and Zirnbauer M R 1997 *Phys. Rev. B* **55** 1142
[37] Peeters C, Hodge T, Mascot E and Rachel S 2024 *Phys. Rev. B* **110** 214506
[38] del Pozo F, Herviou L, Dmytruk O and Le Hur K 2025 *Phys. Rev. B* **111** 075170
[39] Zakharov V A, Fulga I C, Lemut G, Tworzydło J and Beenakker C W J 2025 *New J. Phys.* **27** 033002
[40] Paudel P P, Smith N O and Stanescu T D 2025 *Phys. Rev. Appl.* **23** 034068
[41] Pan H N and Das Sarma S 2024 *Phys. Rev. B* **110** 075401
[42] Liu T, Yan H Y and Guo H 2017 *Phys. Rev. B* **96** 174207
[43] Liu T, Cheng S J, Guo H and Gao X L 2021 *Phys. Rev. B* **103** 104203
[44] Zhang X H, Wilson J H and Foster M S 2025 *Phys. Rev. B* **111** 024207
[45] Peng Y and Refael G 2018 *Phys. Rev. B* **98** 220509
[46] Tezuka M and Kawakami N 2012 *Phys. Rev. B* **85** 140508
[47] Cai X M 2021 *Phys. Rev. B* **103** 214202
[48] Roy K, Roy S and Basu S 2024 *Sci. Rep.* **14** 20603
[49] Ganeshan S, Sun K and Das Sarma S 2013 *Phys. Rev. Lett.* **110** 180403
[50] Lang L J and Chen S 2012 *Phys. Rev. B* **86** 205135
[51] Cai X M, Lang L J, Chen S and Wang Y P 2013 *Phys. Rev. Lett.* **110** 176403
[52] Wang J, Liu X J, Gao X L and Hu H 2016 *Phys. Rev. B* **93** 104504
[53] Aubry S and André G 1980 *Ann. Israel Phys. Soc.* **3** 133
[54] Jitomirskaya S Y 1999 *Ann. of Math.* **150** 1159
[55] Bu X, Zhai L-J and Yin S 2022 *Phys. Rev. B* **106** 214208
[56] Kohmoto M, Kadanoff L P and Tang C 1983 *Phys. Rev. Lett.* **50** 1870
[57] Ostlund S, Pandit R, Rand D, Schellnhuber H J and Siggia E D 1983 *Phys. Rev. Lett.* **50** 1873
[58] Dong J L, Liang E W, Liu S Y, Zhang G-Q, Tang L Z and Zhang D W 2025 *Phys. Rev. B* **111** 174209
[59] Peng D C, Cheng S J and Gao X L 2025 *Phys. Rev. B* **111** 094204
[60] Li S Z, Cheng E H, Zhu S L and Li Z 2024 *Phys. Rev. B* **110** 134203
[61] Biswas S and Chakrabarti A 2024 *Phys. E* **162** 116010
[62] Moustaj A, Kempkes S and Smith C M 2021 *Phys. Rev. B* **104** 144201

[63] Roati G, D'Errico C, Fallani L, Fattori M, Fort C, Zaccanti M, Modugno G, Modugno M and Inguscio M 2008 *Nature* **453** 859
[64] Goblot V, Štrkalj A, Pernet N, Lado J L, Dorow C, Lemaître A, Le Gratiet L, Harouri A, Sagnes I, Ravet S, Amo A, Bloch J, and Zilberberg O 2020 *Nat. Phys.* **16** 832
[65] Kraus Y E and Zilberberg O 2012 *Phys. Rev. Lett.* **109** 116404
[66] Verbin M, Zilberberg O, Kraus Y E, Lahini Y and Silberberg Y 2013 *Phys. Rev. Lett.* **110** 076403
[67] Verbin M, Zilberberg O, Lahini Y, Kraus Y E and Silberberg Y 2015 *Phys. Rev. B* **91** 064201
[68] Kraus Y E and Zilberberg O 2016 *Nat. Phys.* **12** 624
[69] Guo C Y 2024 *Phys. Rev. B* **109** 174203
[70] Liu T 2026 *Int. J. Mod. Phys. B* **40** 2650093
[71] Liu T and Gao X L 2026 arXiv:2605.10746
[72] Liu T and Xia X 2024 *Chin. Phys. Lett.* **41** 017102
[73] Hiramoto H and Kohmoto M 1989 *Phys. Rev. Lett.* **62** 2714
[74] Van Hemmen J L 1980 *Z. Physik B* **38** 271
[75] Zhu J X 2016 *Lect. Notes Phys.* **924** 37
[76] Lieb E, Schultz T and Mattis D 1961 *Ann. Phys.* **16** 407
[77] Kitaev A Y 2001 *Phys. Usp.* **44** 171
[78] DeGottardi W, Sen D and Vishveshwara S 2011 *New J. Phys.* **13** 065028
[79] DeGottardi W, Sen D and Vishveshwara S 2013 *Phys. Rev. Lett.* **110** 146404
[80] Lu Z P, Liu H, Gu Y and Xu Z H 2026 *Chin. Phys. B* **35** 077101
[81] Longhi S 2020 *Opt. Lett.* **45** 4036
[82] Zhang Y C, Yuan R, Song S W, Hu M P, Liu C F and Wang Y J 2025 *Phys. Rev. B* **111** 064201
[83] Zhang P and Nori F 2016 *New J. Phys.* **18** 043033